Superconducting tantalum disulfide nanotapes; growth, structure and stoichiometry.

Charles W. Dunnill[a], Ian Maclaren[b] and Duncan H. Gregory*[a]

Superconducting tantalum disulfide nanowires have been synthesised by Surface Assisted Chemical Vapour Transport (SACVT) methods and their crystal structure, morphology and
10 stoichiometry studied by powder X-ray diffraction (PXD), scanning electron microscopy / energy dispersive X-ray spectroscopy (SEM, EDX), transmission electron microscopy (TEM), selected area electron diffraction (SAED) and nanodiffraction. The evolution of morphology, stoichiometry and structure of materials grown by SACVT methods in the Ta-S system with reaction temperature was investigated systematically. High aspect ratio, superconducting disulfide nanowires are
15 produced at intermediate reaction temperatures (650 °C). The superconducting wires are single crystalline, adopt the 2H polytypic structure (hexagonal space group $P6_3/mmc$: a = 3.32(2) Å, c = 12.159(2) Å; c / a = 3.66) and grow in the $<2\bar{1}\bar{1}0>$ direction. The nanowires are of rectangular cross-section forming nanotapes composed of bundles of much smaller fibres that grow cooperatively. At lower reaction temperatures nanowires close to a composition of TaS_3 are
20 produced whereas elevated temperatures yield platelets of 1T TaS_2.

Introduction

Since the observation of anisotropic nanofibrous inorganic materials in 1979[1] significant interest has developed in the nanostructures of the group 4, 5 and 6 transition metal
25 dichalcogenides. The group 6 disulfide nanotubes, MoS_2 and WS_2, were first characterised in 1992[2] following the discovery of carbon nanotubes by Iijima[3] one year earlier. In the subsequent period, research into the scope of inorganic structures formed by these materials has now grown
30 considerably with a plethora of different inorganic nanofibre, (tubes, rods, ribbons, belts, wires etc) systems known,.[4, 5] For example, the group 6 disulfides, WS_2 and MoS_2, form nanofibres with demonstrable potential as solid lubricants for applications where graphite is not suitable.[2]

35 Tantalum disulfide, TaS_2, like many other transition metal dichalcogenides, exists in a number of different polytypes resulting from the different possible stacking arrangements of the S-Ta-S sandwich layers (in which the metal is typically coordinated in either octahedral or trigonal prismatic
40 geometry to sulphur). These have been much studied and were first described systematically by Jellinek in 1962.[6] The most common polytypes are the 1T, 2H and 3R (single layered trigonal, double layered hexagonal and triple layered rhombohedral respectively) structures (Figure 1) although the
45 6-layer rhombohedral structure, denoted 6R, and 4-layer hexagonal (4H) structure have also been observed with some frequency. Both rhombohedral polymorphs have been described as metastable (kinetically stable at room temperature).[7] The 2H structure thus contains layers of Ta-S
50 trigonal prisms and in the bulk, the 2H form of TaS_2 is metallic with a conduction band that is predominantly metal d_z^2 in character.[8] 2H TaS_2 displays intriguing electronic properties in that it undergoes a transition to a charge density
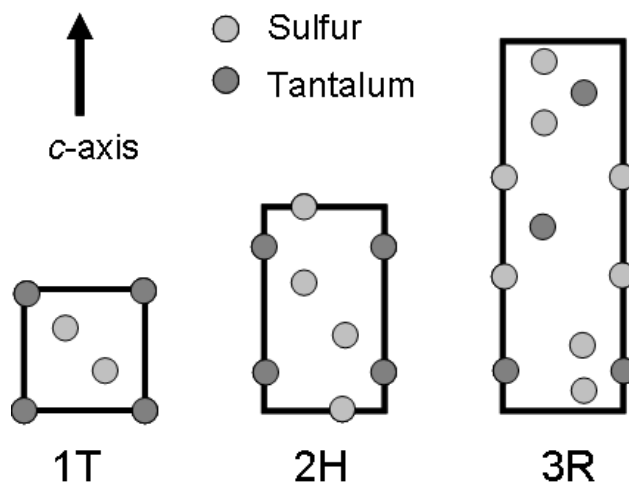
55 **Fig. 1** Schematic illustrating the stacking sequences and coordination in the 1T, 2H and 3R polytype of TaS_2. The structures are shown as projections onto the (110) plane.[6]

wave (CDW) state at 70 K and then a further transition to a superconducting state at 0.8 K.[9] By contrast, the 1T polytype
60 (containing Ta-S octahedra) is non-superconducting at ambient pressure and forms an incommensurate CDW state below 550 K.[10] An important recent development, however, has been the inducement of superconductivity in 1T-TaS_2 at high pressure; the first instance of superconductivity in any
65 1T-structured transition metal dichalcogenide.[11]

In a previous communication we demonstrated that nanowires of tantalum disulfide could be synthesised in a single step Surface Assisted Chemical Vapor Transport process (SACVT).[12] Importantly, the disulfide nanowires that
70 we produced by SACVT were superconducting with an

approximately 5-fold increase in transition temperature compared to that of bulk 2H-TaS_2. The crystal- and precise micro-structure of the superconducting nanowires, however, remain to be determined and these issues have to be addressed if one is to understand the origin of the superconductivity in the nanostructured disulfides. Further, there is a need to understand how these nanowires form and grow and what influence this growth process and the resulting morphology have upon their electronic structure and physical properties.

Here we describe the evolution of morphology, stoichiometry and structure of materials grown by SACVT methods in the Ta-S system with reaction temperature. We demonstrate that high aspect ratio, superconducting disulfide nanowires are produced at intermediate reaction temperatures (650 °C); below this temperature nanowires close to a composition of TaS_3 are produced while at higher temperatures nanowire formation is curtailed and succeeded by formation of characteristic crystalline platelets (with the 1T structure). Importantly, a systematic study of the micro- and crystal structure of the superconducting nanostructures reveals first that the wires are of rectangular cross-section forming nanotapes composed of bundles of much smaller fibers and second that these superconducting disulfide nanotapes are of the 2H polytype.

Results and Discussion

Products of varying morphology were observed under the different reaction temperatures, as shown in Figure 2. Sample **1**, prepared at a final dwell temperature of 400 °C, produced a black polycrystalline powder in region **I** of the ampoules (see experimental section and reference 12), but yielded no nanofibrous material in region **II** (or region **I**), indicating that 400 °C was below the required temperature for formation of nanowires. The black powder in region **I** was identified as a mixture of both the 2H and 3R polytypes of TaS_2 plus the starting materials by the comparison of PXD data with patterns from structures on the ICDD PDF database.[6,13,14] By contrast, sample **2** (500 °C) produced nanofibres that were ribbon-like in appearance and gave a PXD pattern unlike the other materials synthesised at lower or higher temperatures. EDX analysis indicated a higher sulfur content (Ta:S ratio of 1:3) and hence the likely presence of TaS_3. The PXD pattern of **2** however was neither a good match to that calculated from the single crystal structure of monoclinic TaS_3,[15] nor could it be indexed to the earlier reported orthorhombic form of the trisulfide (for which no refined crystal structure is known),[6] possibly eluding to a new phase. TaS_3 is known to be thermodynamically stable at lower temperatures and thermally decomposes at higher temperatures into TaS_2.[16] The stoichiometry and crystal structure of **2** is currently under further investigation. Product **3** took the form of high aspect ratio nanowires and as the main focus of this paper, is discussed in more detail below. Products **4** and **5** prepared with upper dwell temperatures of 750 °C and 900 °C respectively were formed as low yields of nanofibrous material, nucleating in small, isolated clusters on the foil substrate. These fibrous products were of a fine, feathered
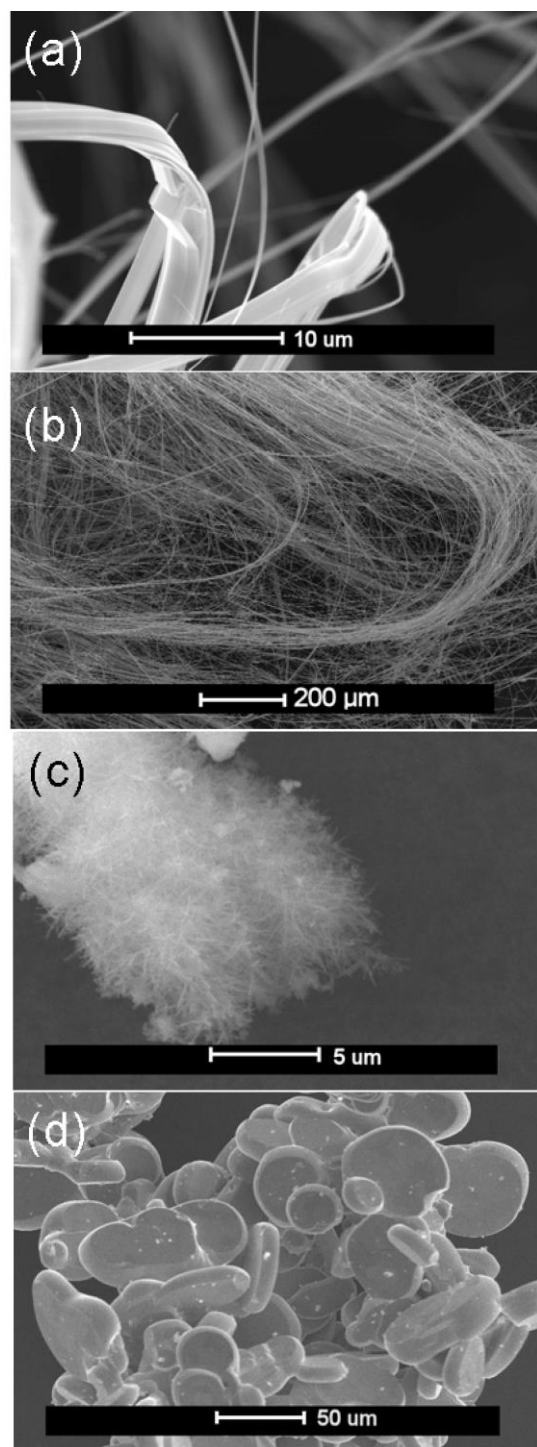

Fig. 2 SEM micrographs of : (a) Nanoribbons (**2**) formed at 500 °C, (b) High aspect ratio nanowires (**3**) formed at 650 °C, (c) Fine nanowires (**5**) formed at 900 °C and (d) platelets (**6**) formed at 1100 °C (recovered from region **I** of the ampoule).

appearance and again yielded an EDX Ta:S ratio of 1:2. Reaction **6** showed no evidence of nanofibrous material in region **II** of the ampoules, and given also the low yields of fibrous material in **5**, suggests that the thermal stability of these materials could lie close to 900 °C. The PXD patterns of the powders recovered from region **I** of these ampoules heated at 1100 °C (Figure 3) show a good match to the 1T polytype
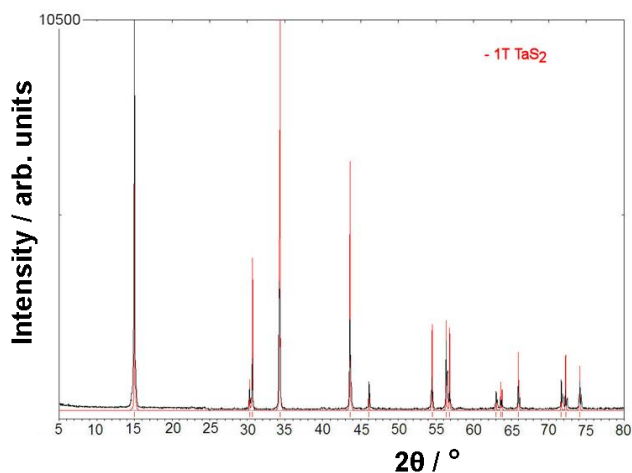
Fig. 3 PXD pattern for the platelets (**6**) formed at 1100 °C showing a match to the pattern calculated from the structure of the 1T polytype of TaS$_2$ (red).
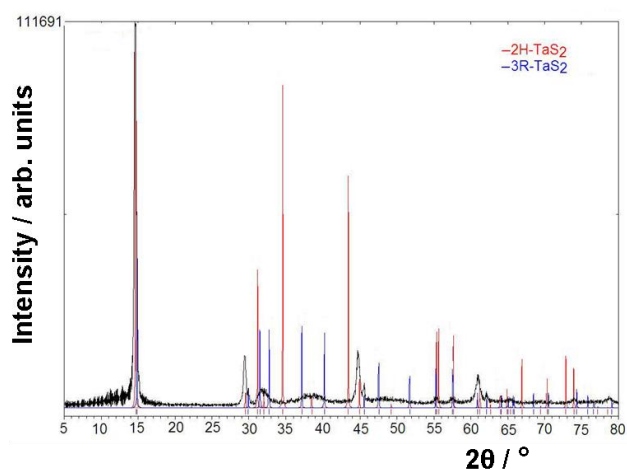

Fig. 4 PXD pattern for **3** with comparisons to the calculated patterns generated from the 2H (red) and 3R (blue) polytype structures.

of TaS$_2$ which has been previously reported as the stable and prevalent high temperature phase at this composition in the Ta-S binary phase system.[7] SEM micrographs reveal products from **6**, region **I** to be well defined platelets of the order of 10-50 μm across (Figure 2d).

Figure 2b shows typical fibres formed at 650 °C (**3**) under the conditions described in the experimental section. Unsurprisingly given their morphology, the nanowires exhibit extreme *00l* preferred orientation, but PXD data (Figure 4) demonstrate that **3** is TaS$_2$. The patterns can be fit approximately to more than one of the possible polymorphs, but most convincingly to either the 2H or 3R structures. In fact, the best refined cell parameters were obtained when the PXD reflections were indexed to the 2H structure, yielding values of *a* = 3.32(2) Å and *c* = 12.159(2) Å; *c* / *a* = 3.66. This represents an expansion along *c* of *ca*. 0.5 % compared to single crystals of ("bulk") 2H-TaS$_2$ (*a* = 3.314(1) Å, *c* = 12.097(1); *c* / *a* = 3.65).[17]

Nath and Rao[18] previously described the possible preference for nano*tubes* of TaS$_2$ to form with the 2H structure on the basis of PXD patterns, however
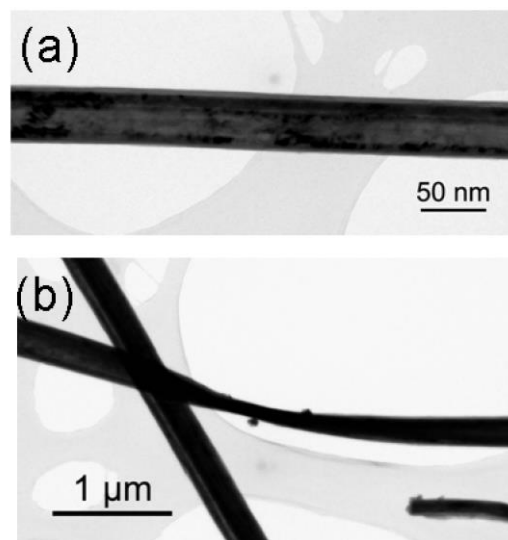

Fig. 5 Bright field TEM image of a section of TaS$_2$ nanowires (**3**): (a) typical flat wire; (b) twisted wire.

differentiation of the polytypes by PXD alone can be difficult and inconclusive given the similarities in the crystal structures and, for example, the tendency for the nanocrystallites to align and exhibit preferred orientation (along the [00l] direction). SEM images (Figure 2b) confirmed the extremely anisotropic morphology of the samples prepared at 650 °C; **3** forms wires exhibiting exceptionally high aspect ratios (typically > 50,000:1), lengths in excess of 3 mm and widths of 50-500 nm. The stoichiometry from EDX was seen to be 36:64(2) (taken from spot scans across multiple regions of several samples). This equates, within error, to the expected 33.3:66.7 (1:2) Ta:S ratio for TaS$_2$ but nevertheless raises the possibility of metal (or sulphur) non-stoichiometry (e.g. Ta$_{1+x}$S$_2$). One also needs to consider, however, the inherent errors of EDX performed on samples of non-uniform (surface) morphology. EDX results from samples from the other reactions yielded similar elemental ratios in all cases for nanofibrous products with the exception of **2** as described above. SQUID data for **3** show a superconducting transition at 3.4 K and as previously outlined (see ESI).[12] Of the bulk TaS$_2$ phases, only the 2H and 6R polytypes are superconducting at ambient pressure (T$_c$ = 0.8 K and 2.3 K respectively)[9,19] which might suggest initially that the likelihood is that the nanowires adopt one of these two polytypic structures. Notably also, nanobelts with the 6R structure are reported to superconduct at 2.7 K,[16] while bulk 6R TaS$_2$ has a T$_c$ > 4 K at 17.3 kbar[19] and bulk 1T TaS$_2$ (non-superconducting at ambient pressure) becomes superconducting with T$_c$ = 6 K at 1 GPa and above, as discovered very recently.[11]

Figure 5a shows a bright field TEM image of a section of a typical TaS$_2$ nanowire from sample **3**. A rather more atypical case is shown in Figure 5b where a wire is twisted and shows a rather thin section at the centre where the lateral width of the wire is small, although the thickness in the beam direction is clearly fairly large, since this section is barely electron transparent. TEM investigations revealed that typical individual nanowires were of the order of 100 - 500 nm across. An SAED pattern from this nanowire in shown
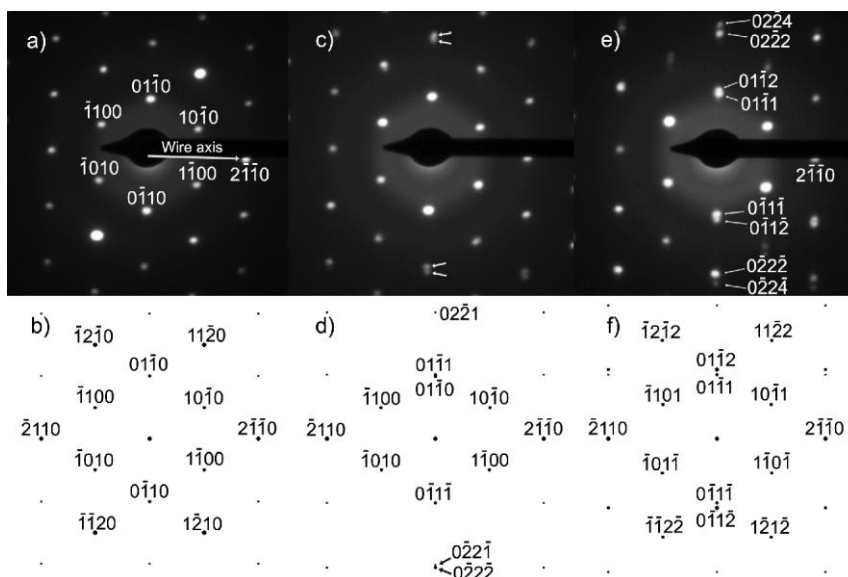
Fig. 6 Image and diffraction patterns of a TaS$_2$ nanowire (**3**): (a) SAED pattern at 0° tilt; (b) simulated [0001] diffraction pattern; (c) SAED pattern after a 10° tilt about the wire axis; (d) simulated 10° tilt pattern; (e) SAED pattern after a 20° tilt about the wire axis; (f) simulated 20° tilt pattern.

in Figure 6a and may be indexed as a [0001] zone axis pattern, as is also shown in the simulation of Figure 6b. Since the rotation between the image and the diffraction modes in the TEM is well known, it was straightforward to determine that the long axis of the crystal runs along one of the $\frac{1}{3}\langle 2\bar{1}\,\bar{1}0\rangle$ crystal directions. Unfortunately, the 1T, 2H, and 3R phases of TaS$_2$ all produce almost identical diffraction patterns along [0001] and this pattern cannot be used to distinguish between the polytypes. The ideal solution would be to have the crystal oriented along a direction in the basal plane, since then the periodicity in the *c*-direction could then be directly determined from the diffraction patterns, but this orientation could not be achieved in the samples mounted on carbon films, except possibly in some cases where the wire was too thick to remain electron transparent.

For this reason, the nanowire was tilted about its long axis in 10° steps. After a 10° tilt, a pronounced spot splitting is observed in the direction perpendicular to the wire axis (arrowed in Figure 6c). Comparisons with a diffraction pattern simulated for the 2H polytype tilted 10° about [$2\bar{1}\,\bar{1}0$] (Figure 6d) result in indices for these split spots of $022\bar{1}$ and $022\bar{2}$ in one direction, and $02\bar{2}1$ and $02\bar{2}2$ in the other. If attempts are made to index these spots for the 1T or 3R polytypes, the only outcome is to obtain fractional indices, i.e. $022\frac{1}{2}$ / $02\bar{2}\frac{1}{2}$ for 1T and as $022\frac{3}{2}$ / $02\bar{2}\frac{3}{2}$ for 3R. This clearly rules out any match to the 1T or 3R phases. The 6R phase would produce additional split reflections, which are not seen, and this possibility can therefore also be excluded.

After a 20° tilt a more pronounced spot splitting is observed between $01\bar{1}1$ and $01\bar{1}2$, as can be seen in Figure 6e and in the simulated diffraction pattern in Figure 6f. As above, the $01\bar{1}1$ spot is only explicable for the 2H structure, as fractional indices result for the 1T or 3R structures in the *c* direction. Thus, electron diffraction in the transmission electron microscope provides unequivocal

evidence that the wires are formed with the 2H structure.

Of the 5 samples prepared in the TEM encapsulation experiments, two successfully exhibited the cross-section of an isolated nanotape within the electron transparent region. Although the SAED data above showed conclusively on tilting that the nanofibres form with the 2H structure without the need for encapsulating samples, the data from the encapsulated samples of **3** did prove interesting. Figure 7a shows a cross-section of a nanofibre. The rectangular shape is clearly observed and it was noted that the general width is about 3 times that of the breadth, leading to nanotape like morphology. Figure 7b shows a nanofibre with an apparently square section with an inset diffraction pattern which was indexed as the [$4\bar{8}43$] zone axis of the 2H structure. This zone axis lies at an angle of ~42° to the [$1\bar{2}10$] direction (the closest direction in the basal plane), so it would have required a large and probably unreachable tilt to orient the ribbon into a position where diffraction from (0002) planes could have been observed directly (the maximum achievable tilt in this microscope is ~40°). It is also likely that the thickness along this direction would have prevented the collection of a diffraction pattern of any quality. Unfortunately, from an assessment of either image it is difficult to construct a complete picture of the three dimensional morphology of the tape, but it is clear that both images are consistent with a flat-topped and flat-sided nanotape morphology, as is set out in more detail below.

TEM observations as shown in Figure 5 and Figure 7, together with SEM observations would appear to suggest that the wires exhibit a thin ribbon- or a tape-like morphology, as shown in Figure 8. The thinnest dimension of the tapes is that parallel to the long *c*-axis, or in other words, the slowest growth is likely to occur perpendicular to the basal plane layers of the 2H structure. The long axis of the tapes is along $\frac{1}{3}\langle 2\bar{1}\,\bar{1}0\rangle$, while the wider dimension is along $\langle 0\bar{1}10\rangle$. It is interesting to note that the nanotapes appear to have a
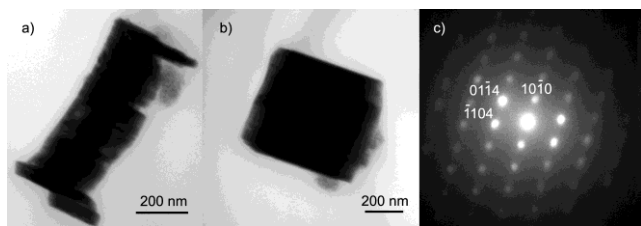
Fig. 7 (a) TEM micrograph showing the cross-sectional area of a nanowire (**3**); (b) square projection nanotape (probably tilted at about 45°); (c) nanodiffraction pattern taken from a thin edge of the particle shown in (b) at zero tilt.

radically different morphology to the hexagonal symmetry of the 2H unit cell (i.e. to the hexagonal space group in which they crystallise). It seems likely that the formation of elongated tapes rather than hexagonal platelets is therefore driven by kinetic or materials supply factors in the synthesis and clearly cannot merely represent a thermodynamically preferred state. Uninhibted growth from a nucleation point in two (or three) dimensions would be expected to yield branched structures (by analogy to snowflakes) that propagate in all six equivalent directions. By contrast growth from a surface would constrain such propagation to one direction only (by analogy to frost, for example, which also typically grows along $\frac{1}{3}\langle 2\bar{1}\bar{1}0\rangle$ directions). It should be noted that the nanotapes always grow from surfaces, so it is very likely that the tape morphology arises as a result of reaction and nucleation at the interface between the tantalum surface and a transported sulfur-containing phase. The evidence of TaS_3 found at lower reaction temperatures combined with the fact that neither any metal (catalyst) particles were added nor were found at the tips or elsewhere of the nanotapes, would suggest that growth occurs *via* a vapour-solid (VS) process involving a sulphur-rich vapour phase and the tantalum foil surface. Such VS growth mechanisms have been proposed for a number of transition metal monosulfides,[20] although in the SACVT experiments described herein, there is no evidence of the tip growth often induced by nanoparticular catalysts (which can often insinuate a vapour-liquid-solid, VLS, process). The accumulated evidence thus points to VS-mediated root growth of the nanotapes from the tantalum substrate surface.

Considering the internal structure of the tapes, it was notable that a significant number of these exhibited a "fibrous" composition, as is exemplified by the nanotape shown in Figure 9. The typical tape morphology is apparent, but dark field images show that the sample is in fact composed of three parallel crystals aligned along the length of the wire. A combination of selected area diffraction, nanobeam diffraction and dark-field imaging showed a few key points. First, all three of the component crystals in the tape grew parallel to [$2\bar{1}\bar{1}0$], consistent with other results, but only the *outer crystals* had the [0001] orientation as the wire sat on the support (shown by the strong diffraction spots in Figure 9d). Second, the weaker diffraction spots in this figure come from the central crystal and this appears to have an orientation close to [$0\bar{2}\bar{2}1$]. Third, tapes of a similar nature that were composed of two or more nanocrystals with a fibrous morphology and a clear [$2\bar{1}\bar{1}0$] fibre texture were

also often observed. These observations would thus suggest that the nanotapes are predominantly if not routinely composed of smaller, fibrous single crystals and would
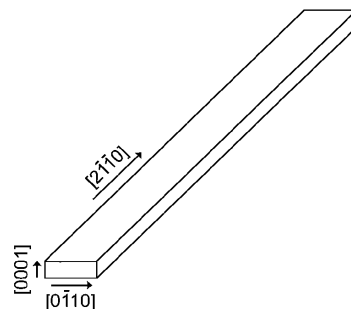

Fig. 8 Schematic diagram of the morphology adopted by the TaS_2 nanotapes (**3**).

suggest that the "bundling" of these smaller fibrils into nanotapes is part of a cooperative growth process. It remains to be established if this "bundling" process is key to the origins of enhanced superconductivity in the $2H$-TaS_2 nanotapes, although similar apparent effects have been described for semi-conducting boron carbonitride nanotubes, which become metallic on forming ordered bundles and also for metallic single walled carbon nanotubes, which on forming such arrays become superconducting.[21,22] Equally, the suppression of charge density waves (CDW) in (bulk) layered dichalcogenides has been an important ingredient in the transition from semiconductivity to superconductivity. The progressive intercalation of copper in $2H$-Cu_xTaS_2 has demonstrated how superconductivity and CDW suppression in dichalcogenides is not only sensitive to carrier concentration and the density of states (DOS) but also and perhaps more importantly, to likely changes in the interaction between Ta-S layers and hence a disruption of the periodicity that induces CDWs.[23] Similar relationships exist in the $2H$-Na_xTaS_2 system[24] and small variations in doping level have commensurate effects on the crystal structure (increases in unit cell volume and expansion along the c direction and a measureable effect for Cu_xTaS_2; $0 \leq x \leq 0.12$ vs. an extremely subtle one in Na_xTaS_2; $0 \leq x \leq 0.1$). In fact, a recent combined computational - single crystal experimental study of the electronic structure and properties of $2H$-$Cu_{0.03}TaS_2$ compared to $2H$-TaS_2, demonstrates that on doping, the area of the Fermi surface increases (along with the value of E_F and the number of charge carriers).[25] While the DOS at E_F decreases in $2H$-$Cu_{0.03}TaS_2$ compared to $2H$-TaS_2, these factors have the combined effect of suppressing the CDWs (reducing the CDW transition temperature), and increasing the superconducting pairing (increasing T_c).

The ostensible connectivity between "chemical" and physical pressure (manifested as substitutionally induced modification of electronic structure, e.g. *via* hole doping) has been documented in high T_c cuprates (converting a Mott insulator ground state to a superconducting state). By loose analogy, pressure has been shown to suppress the CDW ground state in $1T$-TaS_2 to induce superconductivity.[11] Similar pressure-induced effects were observed over a decade ago in the 6R polytype of TaS_2 where T_c could be elevated from 2.3
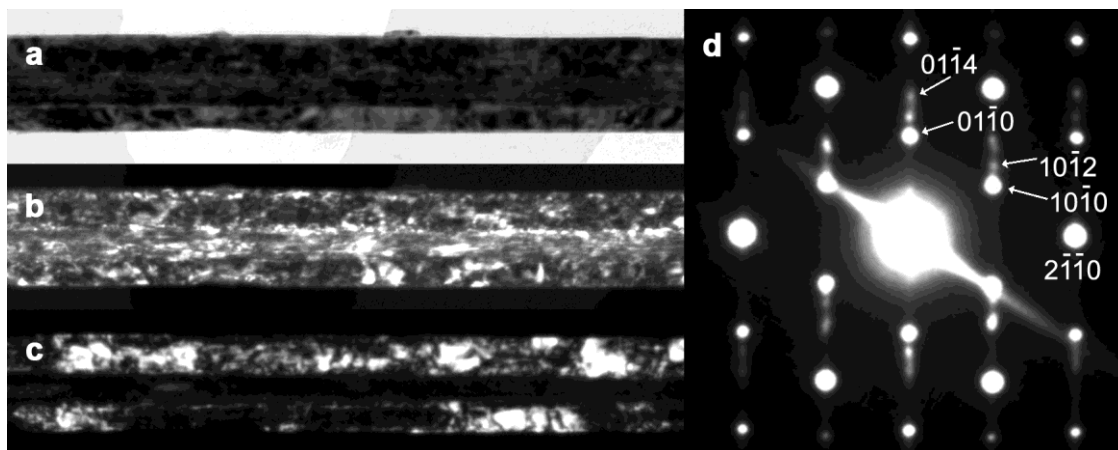
Fig. 9 Images of the internal structure of a nanotape composed of three parallel crystals: (a) Bright field image; (b) Dark-field image obtained using a reflection common to all crystals; (c) Dark field image obtained using a reflection unique to the outer crystals, leaving the central strand dark; (d) selected area diffraction pattern from this nanotape showing a superimposed diffraction pattern of both [0001] and [$0\overline{2}21$] components, together with some reflections generated by double diffraction. The diagonal streaking is a camera artefact from the overexposed transmitted beam.

K at ambient pressure to < 4 K at 17.3 kbar.[19] Just as with doping in 2H-Cu$_{0.03}$TaS$_2$, an increase in pressure in 6R-TaS$_2$ was proposed to increase the area of the Fermi surface and an increase in Cooper pairs. An analogous effect may also be responsible for the observation of elevated T$_c$s in nanowires and nanotubes of NbSe$_2$[26] for which electronic structure calculations have predicted a high DOS at the Fermi level (dominated by Nb 4d states).[27] Importantly, similar calculations have predicted broadly equivalent effects for nanostructured 2H-TaS$_2$ and the likelihood of superconductivity.[28] At present the experimental band structure and DOS of TaS$_2$ nanostructures are unknown. A systematic investigation of the crystal chemistry, electronic structure and transport (and magnetic) properties of individual and bundled dichalcogenide nanowires is essential if we are to establish the equivalent structure-property relationships that are now emerging among the superconducting bulk chalcogenides. An understanding of growth and structure at the nanoscale is a vital first step towards this and to an ability to design chalcogenide nanowires with predictable properties.

Experimental Section

In a typical reaction, elemental powders of tantalum (99.9 %, -325 mesh, Aldridge) and sulfur (99.5 %, Fisher) were ground together in a 1:2 molar ratio and sealed in a 12 mm diameter silica tube under a vacuum of 4x10^{-5} Torr. The tube was modified to accommodate a central constriction effectively dividing the ampoule into two sections (figure 10). One region (**I**) was filled with the reactant powders, the other (**II**) contained a piece of tantalum foil (10 mm x 30 mm x 0.25 mm, 99.9 %, Aldridge).[12] The tube was placed horizontally in a box furnace and heated, first to 115 °C to ensure vaporisation of sulphur and then to temperatures ranging from 400 °C - 1100 °C for 60 - 70 h (Table 1).

The ampoules were subsequently air-quenched to room temperature and opened. Powders in region **I** remain physically separated from products grown on the surface of the foil in region **II**. The latter were mechanically harvested

Table 1 Samples and respective reaction temperatures

Sample Number	Dwell Temperature / °C
1	400
2	500
3	650
4	750
5	900
6	1100

from the foil and retained for analysis. Powder X-ray diffraction, (PXD), analysis was carried out using a Siemens D5000 powder diffractometer in Bragg-Brentano, flat plate geometry. Nanowire samples from region **II** were loaded onto a flat glass disk using a double-sided circular carbon tab, normally used for attaching scanning electron microscopy (SEM) samples to aluminium stubs. Diffraction data were collected between 5 ° ≤ 2θ ≤ 80 ° as a step scan with a 0.02 ° step size over a scan time of 12 h with the sample stage rotating at 15 RPM. High anisotropy and resulting preferred orientation (coupled with crystallite size broadening effects) generally lead to variable quality results from PXD analysis of nanofibrous samples. Many alternative methods of loading samples were attempted with best results obtained from the method described above. PXD data were compared with calculated patterns generated from literature structural data using POWDERCELL and indexed using DICVOL.[29,30]
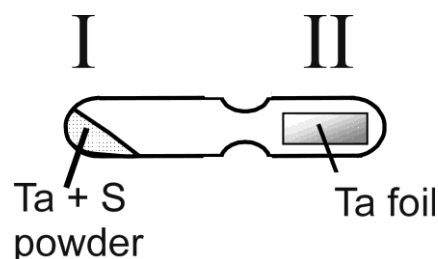

Fig. 10 Schematic diagram of the reaction ampoule, indicating the two discrete sections of the tube.

SEM was performed using a Philips XL30 ESEM. Samples

were loaded onto aluminium stubs using adhesive carbon tabs and imaged in high vacuum mode with an applied 20 kV accelerating voltage and a working distance of 10 mm for energy dispersive X-ray analysis, (EDX). EDX analysis was performed using an Oxford instruments EDX spectrometer in order to determine elemental compositions (which can be obtained with accuracy for elements of atomic number from carbon upwards). Characterisation *via* transmission electron microscopy (TEM) comprised bright and dark field imaging, together with selected area electron diffraction (SAED) and was performed using a FEI Tecnai T20 (FEI Company, Eindhoven, Netherlands) operated at an accelerating voltage of 200 kV. For most measurements, samples were dispersed in isopropanol, and applied dropwise onto a holey carbon film supported on a 300 mesh copper grid. In separate experiments, samples were aligned in the microscope to attempt to image a cross-section of the anisotropic nanowires. For these sample preparations (encapsulations), silicon wafer sheets of 0.6 mm thickness were cut into 10 x 5 mm tabs and cleaned by sonicating in ethanol for 1 min. Epoxy resin infused with nanowires was used to bind the wafers together to form sandwiches which were ground down using wet and dry paper, such that the wafer sandwiches could be arranged vertically in
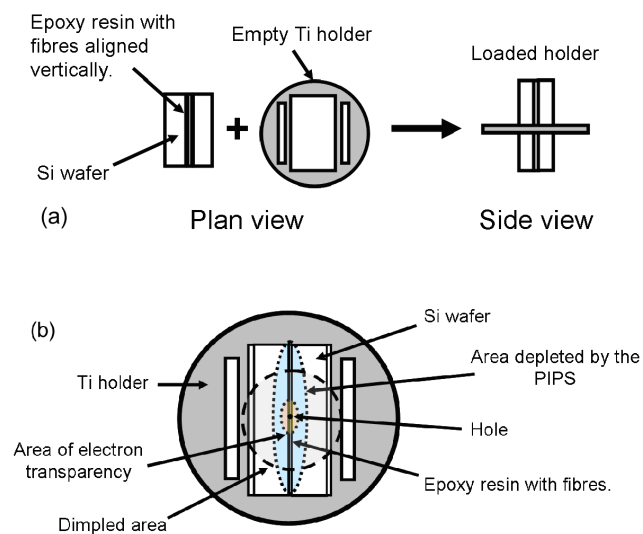

Fig. 11 (a) Schematic of a silicon wafer/epoxy resin sandwich as it is loaded into the titanium sample holder prior to grinding flat for TEM; (b) plan view of an encapsulated sample prepared for a typical TEM experiment to image the cross-section of nanowires.

the centre of titanium encapsulation holders (Technoorg Linda, Budapest, Hungary; Figure 11a). The bound wafers were then ground (with the wafer/epoxy sandwich in a vertical position) until the sandwich (containing the sample) was flush with the surfaces of the flat sample holder (a thickness of *ca.* 80 μm). Dimpling from both sides using a Gatan dimple grinder with 4μm diamond paste to a depth of 35 μm gave a central region of about 10 μm thickness which was further thinned using a precision ion polishing system, (PIPS) until a small hole first appeared in the centre of the wafer sandwich as shown in Figure 11b. Images and diffraction patterns for all

TEM experiments were recorded using an attached SIS Megaview III CCD camera (Olympus Soft Imaging Solutions GmbH, Münster, Germany). Diffraction patterns were simulated using the Desktop Microscopist software package (Lacuna Laboratories, formerly of Beaverton, Oregon, USA.

Magnetic measurements were performed using a Quantum Design MPMS 5T SQUID magnetometer. Samples (~ 20 mg) were loaded into degassed gelatine capsules. Field cooled (FC) and zero field cooled (ZFC) measurements with an applied field of 10 Oe between 1.8 - 20 K. All magnetic data were corrected for the gelatine capsules and for core diamagnetism.

Conclusions

The synthesis of TaS_2 nanotapes has been achieved by a simple one-step reaction from elemental powders *via* SACVT methods in a controllable and reproducible manner. Investigations into the varying composition, structure and morphology of tantalum sulfides with synthesis temperature in SACVT reactions have demonstrated that trisulfide nanomaterials (TaS_3) are obtained at low temperature (e.g. 500 °C) in preference to the disulfide nanostructures seen at 650 °C and above. These reactions at 500 °C produce TaS_3 nanoribbons with high width to thickness ratios and powder XRD patterns that do not correspond to the monoclinc form of TaS_3. Higher reaction temperatures produce nanotapes, fine nanowires and platelets of TaS_2 respectively as the temperature increases and the disulfide progresses through a 2H to 1T phase transition in the process. The nanostructures formed at 650 °C are superconducting below 4 K and TEM confirm that these have the form of nanotapes with $\frac{1}{3}\langle 2\bar{1}\bar{1}0\rangle$ long axes, and [0001] as the narrow tape direction. Further SAED shows unequivocally that the nanotapes are of the 2H polytype, grow in the $\langle 2\bar{1}\bar{1}0\rangle$ and are composed of many smaller fibrils that propagate cooperatively. The modified coupling of Ta-S layers in these nanotapes compared to bulk 2H-TaS_2 is likely to be at the heart of the enhanced superconductivity observed in the nanostructured disulfide.

Notes and references

a WestCHEM, Department of Chemistry, Joseph Black Building, University of Glasgow, Glasgow G12 8QQ, UK. E-mail: D.Gregory@chem.gla.ac.uk
b Department of Physics & Astronomy, Kelvin Building, University of Glasgow, Glasgow G12 8QQ, UK E-mail: I.Maclaren@physics.gla.ac.uk

1 R. R. Chianelli, E. Prestridge, T. Pecorano, and DeNeufville, *Science*, 1979, **203**, 1105.
2 R. Tenne, L. Margulis, M. Genut, and G. Hodes, *Nature*, 1992, **360**, 444.
3 S. Iijima, *Nature*, 1991, **354**, 56.
4 C. N. R. Rao, F. Deepak, G. Gundiah, and A. Govindaraj, *Progress in Solid State Chemistry*, 2003, **31**, 5.

5   M. Remskar, *Adv. Mater.*, 2004, **16**, 1497.

6   F. Jellinek, *J. Less-Common Metals*, 1962, **4**, 9.

7   F. J. DiSalvo, B. G. Bagley, J. M. Voorhoeve, and J. V. Waszczak, *J. Phys. Chem. Solids*, 1973, **34**, 1357.

8   P. Blaha, *J. Phys. Condens. Matter* **1991**, *3*, 9381..

9   S. Nagata, T. Aochi, T. Abe, S. Ebisu, T. Hagino, Y. Seki, K. Tsutsumi, *J. Phys. Chem. Solids* **1992**, *53*, 1259.

10 J. A. Wilson, F. J. DiSalvo, S. Machajan, *Adv. Phys.* **1975**, *24*, 117.

11 B. Sipos, A. F. Kusmartseva, A. Akrap, H. Berger, L. Forró, E. Tutiš, *Nature Mater.* **2008**, *7*, 960.

12 C. W. Dunnill, H. K. Edwards, P. D. Brown, D. H. Gregory, *Angew. Chem. Int. Ed* **2006**, *45*, 7060.

13 H. E. Swanson, E. Tatge, *National Bureau of Standards* **1953**, *539*, 1.

14 B. E. Warren, J. T. Burwell, *Journal of Chemical Physics* **1935**, *3*, 6.

15 A. Meerschaut, L. Guemas, J. Rouxel, *J. Solid State Chem.* 1981, *36*, 118.

16 X. Wu, Y. Tao, Y. Hu, Y. Song, Z. Hu, J. Zhu, L. Dong, *Nanotechnology* 2006, *17*, 201.

17 A. Meetsma, G. A. Wiegers, R. J. Haange and J. L De Boer, Acta Crystallogr. **C46**, 1990, 1598

18 M. Nath, C. N. R. Rao, *J. Am. Chem. Soc.* 2001, *123*, 4841.

19 E. Figueroa, Y.-K. Kuo, A. Olinger, M. A. Lloyd, L. D. Bastin, S. Petrotsatos, Q. Chen, B. Dobbs, S. Dev, J. P. Selegue, L. E. DeLong, C. P. Brock, J. W. Brill, *J. Solid State Chem.*, 1995, *114*, 486.

20 J. P. Ge, J. Wang, H. X. Zhang, Y. D. Li, *Chem. Eur. J.* 2004, *10*, 3525.

21 X. Blase, J.-C. Charlier, A. De Vita, R. Car, *Appl. Phys. Lett.*, 1997, *70*, 197.

22 M. Kociak, A. Y. Kasumov, S. Gueron, *Phys.Rev.Lett*, 2001, *86*, 2416.

23 K. E. Wagner, E. Morosan, Y. S. Hor, J. Tao, Y. Zhu, T. Sanders, T. M. McQueen, H. W. Zandbergen, A. J. Williams, D. V. West, R. J. Cava, *Phys. Rev. B*, 2008, *78*, 104520.

24 L. Fang, Y. Wang, P. Y. Zou, L. Tang, Z. Xu, H. Chen, C. Dong, L. Shan, H. H. Wen, *Phys. Rev. B*, 2005, *72*, 014534.

25 X. Zhu, Y. Sun, S. Zhang, J. Wang, L. Zou, L. E. DeLong, X. Zhu, X. Luo, B. Wang, G. Li, Z.Yang, W. Song, *J. Phys. Condens. Matter* 2009, *21*, 145701.

26 M. Nath, S. Kar, A. K. Raychaudhuri, C. N. R. Rao, *Chem. Phys. Lett.*, 2003, *368*, 690.

27 V. V. Ivanovskaya, A. N. Enyashin, N. I. Medvedeva, A. L. Ivanovskii, *Phys. Stat. Sol.*, 2003, *238*, R1.

28 A. N. Enyashin, I. R. Shein, N. I. Medvedeva, A. L. Ivanonskii, *Internet Electron. J. Mol. Des.*, 2005, *4*, 316, http://www.biochempress.com.

29 G. Nolze, W. Kraus, *Powder Diffr.*, 1998, *13*, 256.

30 A. Boultif and D. Louer, *J.Appl Crystalogr.*, 2004, *37*, 724.